AN EXPERIMENTAL STUDY OF MICROWAVE SCATTERING FROM RAIN- AND WIND-ROUGHENED SEAS

Larry F. Bliven and Jean-Paul Giovanangeli

NASA/Goddard Space Flight Center, Wallops Island, VA 23337, USA and

Institut de Mécanique Statistique de la Turbulence, Marseille, France

Abstract. This paper investigates radar cross section (RCS) characteristics of rain- and wind-roughened sea-surfaces. We conducted experiments in laboratory wind-wave tanks using artificial "rain". The study includes light rain-rates, light wind-speeds, and combinations of these. A 36 Ghz scatterometer was operated at 30 degrees incidence angle and with vertical polarization. RCS data were obtained not only with the scatterometer pointing up-wind but also as a function of azimuthal angle. We use a scatterometer rain and wind model SRWM-1, which relates the total average RCS in storms to the sum of the average RCS due to rain plus the average RCS due to wind. Implications of the study for operational monitoring of wind in rainy oceanic areas by satellite-borne instruments is discussed.

The *International Journal of Remote Sensing*,
Vol. 14, No, 5, 855-869.

Homepage: bliven2.osb.wff.nasa.gov
Email: bliven@osb.wff.nasa.gov
Office Phone:757-824-1057

1. Introduction

Wind is an important factor contributing to weather and climate, so global monitoring of surface winds over the oceans is desirable. Satellite-borne microwave scatterometers measure power levels of echoes from the sea-surface. The echo strength correlates with sea-surface roughness - particularly small-scale roughness. So any processes that affects sea-surface roughness can modify scatterometer measurements. Since nearly ubiquitous winds roughen the sea-surface, wind vectors can usually be inferred from scatterometer observations. Scatterometer data show (a) that power levels increase as wind speed increases and (b) that power levels from azimuthal scans have maxima when the scatterometer is pointing along the mean wind axis.

From time to time, however, it rains. It is well known that rain modifies microwave propagation in the atmosphere and the effects are commonly described in terms of reflection and attenuation. These processes are well understood and so are not the topic of this investigation because models exist that can be used to upgrade scatterometer wind algorithms. Yet, rain strikes the sea-surface and roughens it. When a drop hits a fluid surface it generates a cavity with a crown, which collapses to form a vertical stalk of water, which subsides to spawn rings of gravity-capillary waves that propagate outward (Worthington (1882), Le Méhauté *et al*. (1987) and Le Méhauté (1988)). If no other processes are involved, these features are all cylindrically symmetric. So it is intuitive that rain-generated sea-surface roughness should increase with rainfall rate R and be azimuthally symmetric. When this is the case, scatterometer power levels will (a) vary as a function of rainfall rate but (b) be independent of the azimuthal direction of observation.

Although rain is a recurrent process, only a few studies have examined scatterometer data to assess rain effects on wind velocity retrieval. Operational scatterometer wind retrieval algorithms are empirical relationships between radar cross-section and wind speed (for example, Schroeder *et al*. (1982)). Because the algorithms were developed for fair weather (for example, Jones *et al*. (1977)), rain might cause unpredictable and unreliable results. Indeed, papers by Moore *et al*. (1982), Hawkins and Black (1983) and Black *et al*. (1985) focus on the atmospheric attenuation of signal power attributable to rain. Even after atmospheric corrections are applied, Black *et al*. (l985) report that the Seasat SASS wind speed estimates are biased (too high at low wind speeds and too low at high wind speeds) during rain. Guymer *et al*. (1981) alluded to the potential importance of surface effects but they did not quantify them. A pioneering laboratory study of rain effects on surface returns was conducted by Moore *et al*. (1979) and those data shows that the relative effect of rain varies with wind speed. Thus rain effects on sea-surface roughness can be significant and need to be included in scatterometer wind-retrieval algorithms.

Similar problems have plagued data interpretation from diverse radar systems. Wetzel (1990) modeled electromagnetic scattering from the splash of rain drops for near grazing viewing angles and he compared the model results to laboratory measurements of backscatter from a splashing drop by Hansen (1986). Space applications with synthetic aperture radars (SARs) have also identified rain effects. For example, Weissman *et al*. (1979) predicted that since 1.2 Ghz microwaves penetrate rain, accurate estimates of wind speed would be obtained during hurricanes. When Seasat SAR images from storm areas became available, something was awry. Fu and Holt (1982) presented images of hurricane Iva, tropical storm Greta and severe tropical storms in the Gulf of Mexico, which suggest heavy-rain attenuation of small-scale sea-surface roughness. Ross (1981) reported similar results from SAR images of regions of the Atlantic Ocean.

The predictions were inaccurate, in part, because the algorithms did not account for rainfall effects on sea-surface roughness. Attenuation of surface gravity waves by rainfall has been studied by Reynolds (1875), Nystuen (1990) and Tsimplis and Thorpe (1989). In addition to gravity effects, a model that includes capillarity effects for modulation of rain waves as a function of long phase has been presented by Kharif *et al*. (1989). Diverse regimes have been produced in models by Manton (1973), Le Méhauté and Khangaonkar (1990).

These anomalies necessitate that measurements guide model development because different regimes exist - sometimes rain enhances scatterometer signals and other times rain attenuates scatterometer signals. Our physical understanding of rain effects on sea-surface roughness is incomplete. However if the modifications are a function of microwave wavelength, perhaps winds and rainfall rates can be inverted from dual frequency scatterometer data. Another approach is to obtain an independent estimate of rainfall rate and apply corrections to data from a single frequency scatterometer. Space-borne radiometers can be used to infer rainfall rates.

For this study, we assume that rain rates are known and wind speed estimates are to be obtained by a single frequency scatterometer. We use a scatterometer rain and wind model (SRWM-1) for light-rains and light-winds, in which the *average* total cross-section is the sum of the average rain component plus the average wind component. Thus, all that is needed to predict scatterometer cross-section for combined conditions are calibrations from exclusively rain and exclusively wind conditions. We present the results of experiments designed to validate this hypothesis.

2. A SCATTEROMETER RAIN AND WIND MODEL

We pose a scatterometer rain and wind model (SRWM-1) for backscatter from an air-water interface in which the total average radar cross section σ_T is expressed as

$$\sigma_T = \sigma_R + \sigma_W \qquad (1).$$

Where σ_R is the average normalized RCS due to rain generated roughness and σ_W is the average normalized RCS due to wind generated roughness. We are not aware of scatterometer data to characterize σ_R. At near grazing angles, σ_R increases with rainfall rate and the relationship is a function of microwave polarization (Hansen, (1984)).

Wind-wave fields are usually symmetric with respect to the axis of the average wind-direction, so the azimuthal variation of σ_W is commonly (Ulaby *et al*. (1982)) described by a three term cosine series as

$$\sigma_W = a_0 + a_1\cos(\Theta) + a_2\cos(2\Theta) \qquad (2).$$

Where a_0, a_1 and a_2 depend on wind speed, angle of incidence and polarization. We follow convention by specifying the azimuthal angle $\Theta = 0$ for the scatterometer pointing up-wind. a_0 is the azimuthally averaged cross-section. a_1 is a measure of upwind-downwind asymmetry and a_2 is the cross-wind modulation.

The coefficients a_0, a_1 and a_2 can be derived as follows

$$a_0 = (\sigma_u + 2\sigma_c + \sigma_d)/4 \quad (3a),$$

$$a_1 = (\sigma_u - \sigma_d)/2 \quad (3b),$$

$$a_2 = (\sigma_u - 2\sigma_c + \sigma_d)/4 \quad (3c).$$

Where σ_u, σ_c, and σ_d represent average normalized radar cross sections for the radar looking in the up-, cross-, and down-wind directions. Observations typically show that σ_u increases monotonically as wind speed increases.

Wind forcing is usually the dominant factor contributing to small scale sea-surface roughness and thus RCS. Wind fields can be characterized by either wind speed u_h at some reference height or by wind friction velocity u_* (a measure of momentum flux from the air to the water). Various empirical relationships relate u_h to u_* by using a drag coefficient function (DCF) for scaling. Many studies have been conducted but no DCF has gained universal acceptance. A comprehensive study by Geernaert (1990) indicates that DCF's that include statistics of short-gravity waves and u_* provide improved correlation between model predictions and observations. Laboratory studies of small-scale waves (10's of cm wavelength) show that the air boundary-layer characteristics change dramatically as the average friction velocity exceeds the minimum phase speed for capillary-gravity waves ((Wu (1969a, 1969b, 1980, 1986), Banner and Melville (1976) and Melville (1977)). The change is attributed to the onset of air-flow separation and small-scale wave breaking; the absence or presence of which is associated with (a) different dominant mechanisms for momentum transfer from the air to the water and (b) different processes controlling dissipation - surface tension and viscosity vs gravity . So a transition occurs at u_* of about 25 cm s^{-1} (u_h 8 to 10 m s^{-1}). The existence of wind regimes in scatterometer vs wind data has been reported by Duncan *et al*. (1974), Woiceshyn *et al*. (1986), and Giovanangeli *et al*. (1990). Liu and Large (1981), using the Large and Pond (1981) DCF that has light- and high-wind regimes, report no significant difference between the correlation of RCS vs u_h and RCS vs u_*. Based upon an analysis of a 14 Ghz scatterometer RCS transect across a sharp sea-surface temperature front, Li *et al*. (1989) suggest that there may exist a universal relationship between RCS and u_*.

We will refer to u_* values less than the minimum gravity-capillary wave phase speed as being in a light-wind regime and higher u_* values as in a high-wind regime. To minimize complicating factors and to simplify the physical interpretation of the experimental results, we limit this investigation to the light-wind regime.

3. METHODOLOGY

At sea, winds are variable and rains are intermittent. So great effort and good fortune are needed to obtain data sets to study rain effects on scatterometer wind algorithms. To mitigate these circumstances, we chose to simulate rain in wind-wave tanks. Laboratory experiments can be used as a guide for development of scatterometer algorithms. This section summarizes the laboratory facilities and instrumentation that we used for that purpose.

3.1 Wind-wave tank facilities

We conducted experiments in two wind-wave tanks. One is at GSFC/WFF and the other is at IMST.

The GSFC wind-wave tank dimensions are 20 x 1 x 1.5 m. Operational water depth is 0.7 m so the air column for wind is 0.5 m. Wind speeds from 0 to 20 m s^{-1} can be produced by a suction fan through a closed-loop recirculation system. For field studies, u_h is typically referenced to a height of 10 m, which is higher than measurement feasibility in wind-wave tanks. u_* is measurable in the laboratory, so we use it to characterize the wind field. We measure wind-speed profiles using pitot tubes and compute u_*. During the experiment, the radar and rain simulator were located about 13 m from the up-wind beach. The radar was only pointed up-wind due to the restrictive width of the tank. We concentrated on the effect of rain at light wind-speeds, so we performed experiments with the following conditions: (a) a range of light winds, without rain; (b) a range of light rains, without wind; and (c) combinations of the light winds and light rains.

The IMST wind-wave tank dimensions are 40 x 3 x 2.5 m and the facility is described in detail by Coantic and Favre (1974). The operational water depth is approximately 1 m so the height of the aerodynamic flow above the water surface is about 1.5 m. The maximum wind velocity is 14 m s^{-1} and friction velocity is computed from hot-wire anemometer data using the covariance method. That is $u_* = \langle -u'w' \rangle^{1/2}$, where <> means time averaged and u' and w' are the longitudinal and vertical air velocity fluctuations. At IMST, the radar and rain simulator were located about 35 m from the up-wind beach. A mechanical device varied the azimuthal angle between wind direction and radar observation from 0^o to 360^o, while keeping constant the incidence angle and the location of the footprint center. A study of the azimuthal response of the scatterometer as a function of wind speed is reported in Giovanangeli *et al*. (1990). For this study, we used the extra wide feature of the wind-tank to study azimuthal variability for (a) a fixed light wind-speed (no rain) and (b) combinations of the light-wind case and several light rains.

3.2 Instrumentation

A 36 GHz (8 mm wavelength) radar system was used at both facilities and a schematic of the radar system has been presented by Bliven and Norcross (1988) and examples of cross section time series data were presented by Bliven *et al*. (1988). We used a standard procedure to calibrate the radar, that is to say, data are normalized relative to the return from a 15 cm diameter metal sphere at 1 m range. We digitized the analog signals from the scatterometer and computed average voltages V^2. We calculated normalized radar cross section σ as the ratio of V^2 to that from a 15 cm diameter metal sphere at the appropriate range. These values can be converted to decibel units according to the formula

$$\sigma_0(\text{dB}) = 10*\log(\sigma) \qquad (4).$$

The scatterometer has operated in both wind-wave tanks at 1 m range to the calm water surface. The alignment was at 30 degrees inclination from nadir and vertical polarization was used for both transmit and receive horns. With this setup, the radar footprint diameter on a calm water surface is approximately elliptical with dimensions of 12 x 10 cm^2.

We built rain simulators to provide rainfall rates and drop sizes similar to natural rain. For the natural environment, rain rate statistics vary with both averaging duration and measurement area,

such that higher maximum values generally corresponding to shorter duration and smaller areas. Typical saturation levels for satellite-based radiometer rainfall rate measurements over the ocean are on the order a few 10's of mm hr^{-1}. For these conditions, drop-sizes typically range from 1 to 3 mm. We constructed a rain simulator to use at NASA that produced uniformly sized 2.8 mm water drops that fell from 10 nozzles (14 x 7 cm spacing). The simulator was located 1.5 m above the water surface and the drops accelerated by gravity to about 3.5 m s^{-1} before striking the water surface. Though the impact speed was only about 50 percent of terminal velocity in air, drops striking the water surface generated vertical stalks as well as surface ripples within the radar footprint. Rainfall rates from 0 to 12 mm hr^{-1} were produced by controlling the water-supply pressure.

For the experiments at IMST, the rain simulator consists of 72 nozzles (arranged in an 8 x 9 grid with 5 cm spacing) distributed among six sizes that generated drops that ranged from 1.2 to 2.8 mm. This rain simulator design has uniform flow rates through all the different sized nozzles - consequently the smaller nozzles produced more drops than the larger nozzles. The drop size distribution of this rain simulator is similar to natural rain, which is often described in terms of a Marshall-Palmer distribution. During the experiments, the IMST rain simulator was located approximately 1 m above the calm water surface and centered over the radar footprint.

4. RESULTS

4.1 Experiments at NASA

Rainfall rate is commonly used to characterize storm intensity so we are interested in knowing how σ_R varies with rainfall rate. Fig. 1 displays data from the NASA experiments in which uniform 2.8 mm diameter drops fell into the water within the radar footprint. The data depict a linear trend so we computed a least-squares linear model which is

$$\sigma_R = 3.3 \times 10^{-3} R(\text{mm hr}^{-1}) \quad (5).$$

The correlation coefficient is greater than 0.95, so a simple linear function is adequate.

The wind-study cross-section measurements, obtained with the radar pointing up-wind, are presented in a logarithmic format in Fig. 2. We employ conventional practice and use a power-law model for the scatterometer wind speed algorithm, i.e.,

$$\sigma_u = G\, u_*^{H} \quad (6).$$

A least squares analysis indicates for u_* in cm s^{-1} that

$$\sigma_u = 2.0 \times 10^{-3}\, u_*^{2.0} \quad (7).$$

The correlation coefficient is 0.98. It is fascinating, but maybe fortuitous, that H is approximately 2; σ_u varies approximately as a quadratic function of friction velocity.

Comparison of the rain data set and the wind data set reveals (a) that σ_u for the lightest wind condition (u_* = 5 cm s^{-1}) is comparable to that of the lightest rain condition and (b) that for the entire light-wind regime, the range is twice as large as measured for light rainfall rates with this NASA rain

simulator. So echoes from these light wind and light rain simulations are of similar magnitude and thus both processes should be important for combined wind and rain simulations.

The combined conditions data set is composed of cross section measurements for all combinations of the light wind and light rain settings and is shown in logarithmic format in Fig 3. First, either processes can dominant, depending upon wind and rain conditions. Consequently, rain effects on scatterometer wind speed algorithms should not be ignored. Next, cross sections are typically enhanced by light rain, so if rain effects are not accounted for in wind retrieval algorithms, wind speed estimates are expected to be biased high. Finally, although cross sections at a given wind speed generally increase with greater rainfall, the relative change decreases as wind speed increases. These primary features are consistent with K_u-band scatterometer data from laboratory experiments (Moore *et al*. (1979)) and the positive bias (over estimate) of light wind speed estimated due to rain (Black *et al*. (1985)) for Seasat field data.

Even with its simple form, SRWM-1 resolves the principal features of the combined data set. For example, by expressing SRWM-1 in logarithmic form we obtain

$$\log(\sigma_T) = \log(\sigma_W) + \log(1+ \sigma_R/\sigma_W) \qquad (8).$$

The terms on the right hand side of Equation 8 represent the traditional cross section due to wind plus a perturbation due to rain. The magnitude of the rain perturbation scales as a function of wind, i.e., there is an apparent interaction. σ_W is an increasing function of wind speed, so for a specified rainfall rate, the rain effect decreases as wind speed increases.

We examined the effectiveness of compensating for rain effects on scatterometer wind retrieval by using SRWM-1. In particular, σ_u values are estimated by computing σ_T - σ_R values. We used the linear empirical model for the NASA simulator to obtain σ_R values from rainfall rates and present the results in Figure 4. Compared to neglecting rain effects, application of SRWM-1 improves friction velocity estimates for combined wind and rain conditions because it greatly reduces the large positive biases.

4.2 Experiments at IMST

We conducted experiments in the large wind-wave tank at IMST to investigate the azimuthal variation of scatterometer echoes due to light rain and light wind. The tank is exceptionally wide, so we placed a high priority on making measurements to quantify the azimuthal variability. These data are presented in this section and they are interpreted using SRWM-1.

A validation study was performed to ensure that acceptable scatterometer data are obtained at various azimuthal angles within the tank. For ideal conditions, scatterometer measurements are expected (a) to be highest in the along-wind axis for wind-roughened water-surfaces and (b) to be independent of azimuthal direction for rain-roughened water-surfaces. The azimuthal variation of σ_W for a light wind-speed in the wind-wave tank is shown in Fig. 5. Data obtained for the entire 360^o's show the usual patterns of (a) along-wind maxima and cross-wind minima and (b) σ_u slightly greater than σ_d. For comparison, the azimuthal variation of σ_R for a light rain from the variable drop-size rain simulator are also shown in Fig. 5. Although σ_R is nearly constant, the data in the direction of the side-walls show a slight increase compared to the data along the wind-axis. Although the asymmetry for the rain case is almost imperceptible, it is real and explainable. Rain ripples diminish as they propagate away from the impact region. We saw this in the tank. In the long axis direction of the tank, the ripples propagate away over great distances and become invisible. In the direction of the sidewalls, however, we could see that they are reflected back. This causes the small and inconsequential asymmetry in the rain data set. Thus we conclude that acceptable scatterometer data are obtained at all azimuthal angles of interest.

The scatterometer azimuthal variation for a light-wind case is shown in Fig. 6 for measurements at 10^{o} increments from the up- to down-wind directions. Again, the pattern of along-wind maxima and a cross-wind minimum is unmistakable.

Combined conditions were investigated for combinations of the light-wind case and several rainfall rates. The data are shown in Fig. 6. At each azimuthal angle, cross section typically increases with increasing rainfall rate. This trend is similar to that of the up-wind data for combined conditions described in the previous section.

We computed σ_R for each rainfall rate by subtracting the azimuthally-averaged cross-section for the wind-only case from the azimuthally-averaged values for the combined cases. The results, which are presented in Fig. 1, are nearly linear. A linear least-square fit of the data shows that

$$\sigma_R = 7.3 \times 10^{-3} R(\text{mm hr}^{-1}) \quad (9),$$

with a correlation coefficient greater than 0.99. For rainfall rates less than about 20 mm hr^{-1}, it appears that a linear relationship between σ_R and rainfall rate is robust.

It is intriguing that the slopes of the linear regressions for the NASA and IMST rain simulators differ by approximately a factor of 2. The IMST simulator is larger and generates multiple drop-sizes to give a better approximation of natural rain. Let's consider the possible effect of size first. The simulator at NASA generated rain entirely within the radar footprint. The simulator at IMST covered an area larger than the radar footprint so rain-ripples propagated not only away from but also into the radar footprint. Results of the azimuthal validation study showed that the scatterometer detects increased surface roughness due to rain-ripples propagating into the radar footprint. So a plausible explanation of the factor of 2 is that for an equivalent rainfall rate, the surface was rougher due to the larger size of the rain simulator. Although the rain simulator size difference is a credible explanation of the slope change, we can not rule out the possibility that the slope changed due to the gross change of drop-size distributions between the NASA and IMST rain simulators. For field conditions, a linear dependence may be satisfactory because natural drop-size distributions do not vary dramatically for rainfall rates less than 25 mm hr^{-1}. Studies of rain drop-size distributions usually show that the Marshal-Palmer distribution is an accurate representation, i.e., drop-size number-density decreases logarithmically as size increases and the median size increases slowly as rainfall rate increases. More experiments are needed to define an operational algorithm. It seems likely, however, that if drop-size distribution is stable, a linear relationship between NRCS and rainfall rate will provide sufficient accuracy for K_a-band scatterometers monitoring light rain rates.

The utility of compensating for rain effects on the scatterometer azimuthal measurements by using SRWM-1 is illustrated in Fig. 7. We computed σ_W from $\sigma_T - \sigma_R$ (using the linear model for the IMST rain simulator to estimate σ_R values from rainfall rates). These results show that the model provides well-behaved results in all directions.

Indeed, a property of SRWM-1 is that rain does not modify a_1 or a_2 values. So we investigated these coefficients as a function of rainfall rate using a least squares method to derive the coefficients. The results are plotted in Fig. 8(a&b), which show the coefficient estimates and standard errors (shown by vertical bars). Also plotted are the group average values of a_1 and a_2 and their variances (shown by horizontal solid and dashed lines). Given the variance of individual estimates relative to the group statistics, a_1 and a_2 do not show a clear or strong functional dependence on rainfall rate. The variability of a_1 and a_2 for the various rain and wind cases is also small compared to the variability reported by Giovanangeli *et al.* (1990) for scatterometer azimuthal response due to light winds. Although further investigations may reveal minor variations, we conclude that for light winds and light rains, a_1 and a_2 are not a strong function of rainfall rate.

These azimuthal experiments corroborate the usefulness of SRWM-1 for light wind and light rain conditions. Although alternate models can always be proposed, SRWM-1 is simple and can be used for practical data inversions techniques to measure wind speed and direction for light wind and rain conditions. For example, this would be a natural extension of the synergic inversion technique for active and passive microwave remote sensing of the ocean proposed by Sobieski *et al*. (1991).

5. SUMMARY AND CONCLUSIONS

These laboratory simulations of scatterometer cross-sections from an air-water interface roughened by light winds and light rain show that to within normal measurement accuracy, rain and wind can be treated as separate processes. So if a scatterometer system is calibrated as a function of wind speed (without rain) and also as a function of rain rate (without wind), then for combined light-rain plus light-wind conditions, cross-section measurements should be predictable. Or from an operational perspective, if rain rates are inferred by an instrument such as a radiometer on a satellite, then it should be possible to reduce biases in wind speeds estimates.

Global wind stresses derived from Seasat scatterometer data can be used to calculate ocean circulation. This was demonstrated by Chelton *et al*. (1990) who used the SASS vector wind observations with directional ambiguities removed by Atlas *et al*. (1987). Generally good results were obtained and the potential for satellite scatterometery to improve and make important contributions to ocean modeling was demonstrated. Nevertheless, even this basic circulation model shows that small biases in wind stress estimates results in significant changes in model outcome. Particular concern was expressed for light wind regions, specifically the tropical oceans.

Rain is an important processes in tropical ocean areas. Indeed, the Tropical Rainfall Measurement Mission report, by Simpson (1988), states that the primary goals of the proposed mission are to measure the vertical distribution of rain in the atmosphere and the rainfall rate. This information is essential to determine where latent heat exchange is occurring and will be used in climate models to provide more accurate heat budget estimates.

Thus particular attention is needed to ensure that scatterometer wind estimates over the Tropical ocean are not biased by rain effects on microwave scattering from the air-sea interface. Naturally, further research is needed because the physics for higher wind speeds and rainfall rates is more complex and unfortunately data are unavailable. This study does, however, provide encouragement that operational algorithms can indeed be improved by including rain-roughening of the sea surface. Consequently, it seems likely that biases attributable to rain roughening of the air-sea interface can be reduced or eliminated in scatterometer wind algorithms.

Acknowledgments

We are grateful to our colleagues at IMST and NASA who participated in this research. In particular, G Norcross provided indispensable technical support with the radar and J Quaccia expedited international equipment shipments. P Twitchell stimulated technical discussions. Sincere thanks are offered to the family of Chester Parsons for his dedicated career with NASA. NASA (RTOP 672-161-80-28) and the Office of Naval Research (ONR 672-146-70-11) contributed funding for this research. The french authors thank also the Centre National de la Recherche Scientifique, the Direction des Recherches, Etudes et Techniques and the PAMOS committee which contributed funding for this research.

REFERENCES

ATLAS, R., BUSALICCHI, A.J., GHIL, M., BLOOM, S., and KALNAY, E., 1987, Global surface winds and flux fields from model assimilation of Seasat data. *Journal Geophysical Res*earch, **92**, 6477-6487.

BANNER, M. L., and MELVILLE, W.K., 1976, On the separation of air flow over water waves. *Journal Fluid Mech*anics, **77(4)**, 825-842.

BLACK, P. G., GENTRY, R.C., CARDONE, V.J. and HAWKINS, J.D., 1985, Seasat microwave wind and rain observations in severe tropical and mid-latitude marine storms. *Advances in Geophysics,* **27**, 198-278.

BLIVEN, L.F., GIOVANANGELI, J-P, and NORCROSS, G., 1988, A study of rain effects on radar scattering from water waves. *Proceedings of the 7th Conference on Ocean-Atmosphere Interactions of American Meteorological Society held in Anaheim, California, on 1-5 February 1988,* Boston, MA: American Meteorological Society D(VT) 500 1/88, 230-233.

BLIVEN, L.F. and NORCROSS, G., 1988, Effects of rainfall on scatterometer derived wind-speeds. *Proceedings of the IGARSS'88 held in Edinburgh, Scotland, on 12-16 September 1988,* ESA SP-284 (Paris: European Space Agency), ***1***, 565-566.

CHELTON, D.B., MESTAS-NUNEZ, A.M., and FREILICH, M.H., 1990, Global wind stress and Sverdrup circulation from the Seasat scatterometer, *Journal Physical Oceano*graphy, **20**, 1176-1205.

COANTIC, M. and FAVRE, A., 1974, Activities in and preliminary results of air- sea interaction research at IMST. *Advances in Geophysics,* **16**, 391-405.

DUNCAN, J.R., KELLER, W.C. and WRIGHT, J.W., 1974, Fetch and wind speed dependence of Doppler spectra. *Radio Science,* **9**, 809-819.

FU, L., and HOLT, B., 1982, Seasat views oceans and sea ice with synthetic-aperture radar. NASA-JPL pub 81-120, 200.

GEERNAERT, G.L., 1990, Bulk parameterizations for the wind stress and heat fluxes. In *Surface Waves and Fluxes, edited by G.L. Geernaert and W.J. Plant (Amsterdam: Kluwer Academic Publishers),* **1**, 91-172.

GIOVANANGELI, J-P., BLIVEN, L.F., and LE CALVE, O., 1990, A wind-wave tank study of the azimuthal response of a Ka-band scatterometer. *I.E.E.E. Journal Geoscience and Remote Sensing,* **29(1)**, 143-148.

GUYMER, T.H., BUSINGER, J.A., BRACALENTE, E.M., DOME, G.J. and WENTZ, F.J., 1981, Evaluation of atmospheric attenuation from SMMR brightness temperature for the SEASAT satellite scatterometer. *Nature,* **294**, 735-737.

HANSEN, J.P., 1984, High resolution radar backscatter from a rain disturbed sea surface. *ISNR-84 Record, Symposium held in Tokyo, Japan, on 22-24 October, 1984.*

HANSEN, J.P., 1986, A system for performing ultra high resolution backscatter measurements of splashes. *Proceedings of the International Microwave Theory and Techniques Symposium*, I.E.E.E., New York.

HAWKINS, J.D. and BLACK, P.G., 1983, SEASAT scatterometer detection of gale force winds near tropical cyclones. *Journal Geophysical Research,* **88(C3),** 1674-1682.

JONES, W.L., SCHROEDER, L. and MITCHELL, J.L. 1977, Air-craft measurements of the microwave scattering signatures of the ocean. *I.E.E.E. Journal Oceanographic Engineering,* **OE 2**, 52.

KHARIF, C., GIOVANANGELI, J-P., and BLIVEN, L.F., 1989, Rain waves-wind waves interaction and application to scatterometry. *Proceedings of IGARSS'89 held in Vancouver, Canada, on 13-16 July 1989*, ESA SP-284 (Paris: European Space Agency), **3**, 1891-1896.

LARGE, W.G., POND, S., 1981, Open ocean momentum flux measurements in moderate to strong winds. *Journal Physical Oceanography,* **11,** 324-336.

LE MEHAUTE, B., 1988, Gravity-capillary rings generated by water drops. *Journal Fluid Mechanics,* **197**, 415-427.

LE MEHAUTE, B. and KHANGAONKAR, T., 1990, Dynamic interaction of intense rain with water waves. *Journal Physical Oceano*graphy, **20**, 1805-1812.

LE MEHAUTE, B., WANG, S., and LU, C.C., 1987, Spikes, domes, and cavities. *Journal International Association of Hydraulic Res*earch, **5**, 583-602.

LI, F., LARGE, W., SHAW W., WALSH, E.J., and DAVIDSON, K., 1989, Ocean radar backscatter relationship with near-surface winds: a case study during FASINEX. *Journal Physical Oceano*graphy, **19**, 342-353.

LIU, W.T. and LARGE, W.G., 1981, Determination of surface stress by Seasat-SASS: a case study with JASIN data. *Journal Physical Oceano*graphy, **11**, 1603-1611.

MANTON, M.J., 1973, On the attenuation of sea waves by rain. *Geophysical Fluid Dyn*amics, **5**, 249-260.

MELVILLE, W.K., 1977, Wind stress and roughness length over breaking waves. *Journal Physical Oceano*graphy, **7**, 702-710.

MOORE, R.K., YU, Y.S., FUNG, A.K., KANEKO, D., DOME, G.J., and WERP, R.E., 1979, Preliminary study of rain effects on radar scattering from water surfaces. *I.E.E.E. Journal of Oceanographic Engineering*, **OE-4(1)**, 31-32.

MOORE, R.K., BIRRER, I.J., BRACALENTE, E.M., DOME, G.J., and WENTZ, F.J., 1982, Evaluation of atmospheric attenuation from SMMR brightness temperature for the Seasat satellite scatterometer. *Journal of Geophysical Research*, **95(C10)**, 3337-3354.

NYSTUEN, J.A., 1990, A note on the attenuation of surface gravity waves by rainfall. *International Journal of Geophysical Research,* **95(C10),** 18353-18355.

REYNOLDS, O. 1875, On the action of rain to calm the sea. *Proceedings of the Literary Philosophical Society of Manchester*, **XIV**, 72-74.

ROSS, D.B., 1981, The wind speed dependency of ocean microwave backscatter, In *Spaceborne Synthetic aperture radar for oceanography*, edited by Beal, R.C., DeLeonibus, P.S., and Katz, I. (Baltimore, MD: The Jonhs Hopkins University Press), 75-84.

SCHROEDER, L.C., BOGGS, D.H., DORNE, G., HALBERSTRAM, I.M., JONES, L.W., PIERSON, W.J. and WENTZ, F.J., 1982, The relationship between wind vector and normalized radar cross section used to derive Seasat A satellite scatterometer winds. *Journal Geophysical Res*earch, **87(C5)**, 3318-3336.

SIMPSON, J. (editor), 1988, Report of the science steering group for a Tropical Rainfall Measuring Mission (TRMM). NASA, 1-94.

SOBIESKI, P., GUISSARD, A., and BAUFAYS, C., 1991, Synergic inversion technique for active and passive microwave remote sensing of the ocean. *I.E.E.E. Transactions on Geoscience and Remote Sensing,* **29(3),** 391-406.

SROKOSZ, M.A., and GUYMER, T.H., 1988, A study of the effect of rain on Seasat radar altimeter data, *Proceedings of the IGARSS '88 Symposium held in Edinburgh, Scotland, on 13-16 September 1988,* ESA SP-284 (Paris: European Space Agency), 651-654.

TSIMPLIS, M. and THORPE, S.A., 1989, Wave damping by rain, *Nature,* **342**, 893-895.

Ulaby, F.T., Moore, R.K., and Fung, A., 1982, *Microwave Remote Sensing*, **II, (**Reading, MA: Addison-Wesley).

WEISSMAN, D.E., D.B. KING, and THOMPSON, T.W., 1979, Relationship between hurricane surface winds and L-band radar backscatter from the sea surface. *Journal Applied Meteorology*, **18,** 1023-1034.

WETZEL, L.B., 1990, On the theory of electromagnetic scattering from a raindrop splash. *Radio Science,* **25(6)**, 1183-1197.

WOICESHYN, P.M., WURTELE, M.G., BOGGS, D.H., MCGOLDRICK L.F., and PETEHERYCH, S., 1986, The necessity for a new parameterization of an empirical model for wind/ocean scatterometry. *Journal Geophysical Res*earch, **91(C2)**, 2273-2288.

Worthington, A.M., 1882, A study of splashes. *Proceedings of the Royal Society of London,* **34**, 217-229.

WU, J., 1969a, Wind stress and surface roughness at air-sea interface. *Journal Geophysical Research*, **74(2)**, 444-454.

WU, J., 1969b, A criterion for determining air-flow separation from wind waves. *Tellus*, **21**, 707- 713.

WU, J., 1980. Wind-stress coefficients over the sea surface near neutral conditions - a revisit. *Journal Physical Oceanography*, **10**, 727-740.

WU, J., 1986, Roughness elements of the sea surface - their spectral composition. *Tellus,* **38(a)**, 178-188.

ULABY, F.T., MOORE, K.M., and FUNG, A., 1982, *Microwave remote sensing,* **II**, (Addison-Wesley Publishing Company).

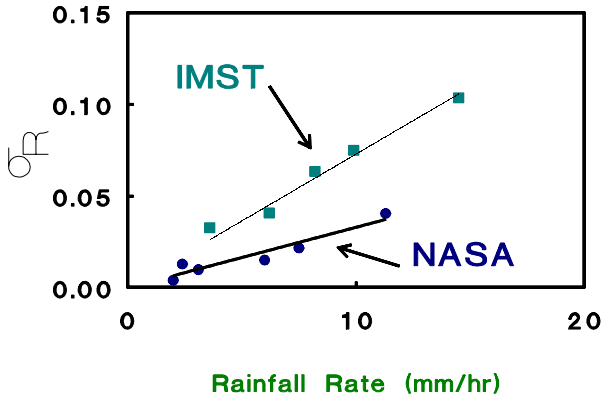

Figure 1. Scatterometer (Ka-band, vv polarized, 30 degrees incidence angle) measurements from an air-water interface *roughened by 'artificial' rains.* The NASA and IMST rain simulators differed in both drop size distribution and areal size. A linear response function is acceptable for each rain simulator.

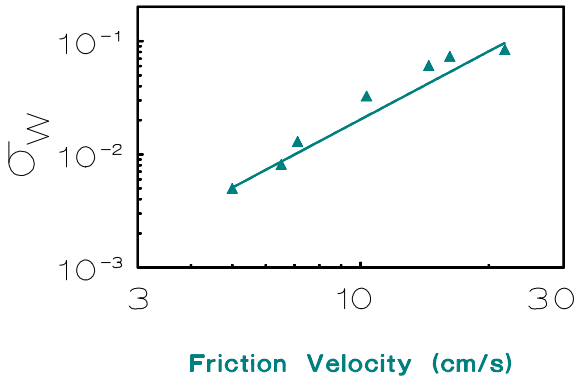

Figure 2. Scatterometer measurements in the up-wind direction from an air-water interface *roughened by light winds.* A least-squares power-law model indicates an approximately quadratic relationship.

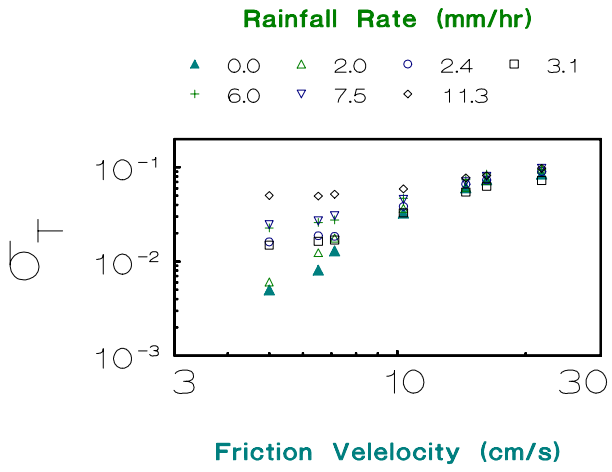

Figure 3. Scatterometer measurements in the up-wind direction from an air- water interface *roughened by light winds and light rains*. The relative effect of rain decreases as wind speed increases. If rain effects are neglected, not only do scatterometer wind estimates worsen as rain rates increase but also a positive bias arises.

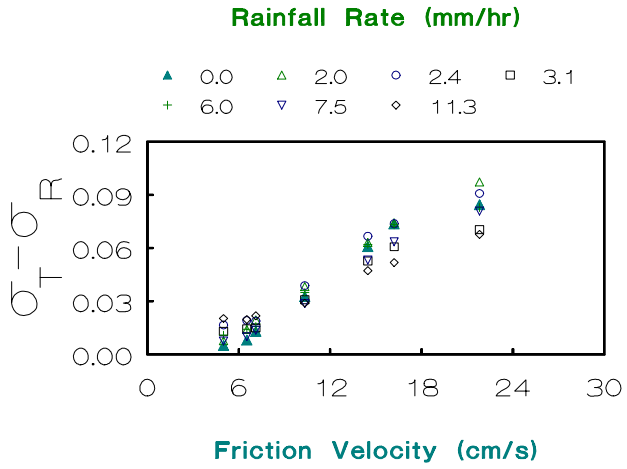

Figure 4. The empirical linear response function for the NASA rain simulator is used in the SRWM-1 model to compensate for rain effects on scatterometer wind speed estimates. Values for wind only cases are shown for comparison. For rainy conditions, up-wind scatterometer wind-speed estimates are feasible using SWRM-1.

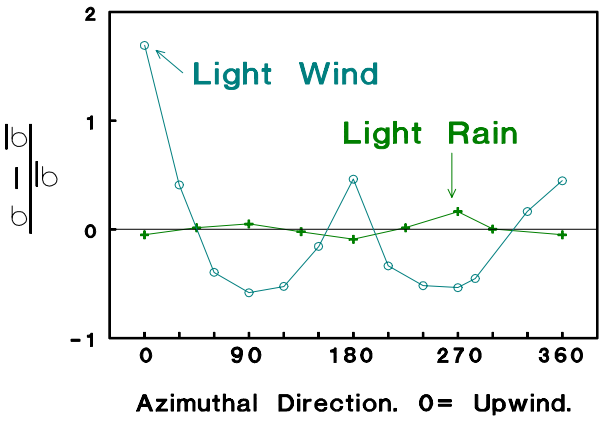

Figure 5. *Azimuthal variations* of NRCS for a nearly isotropic rain-generated wave-field and a wind-generated wave-field. Uniformity of response to rain-generated waves and typical asymmetric response from wind-generated waves demonstrate that azimuthal measurements are possible in the wind-wave tank.

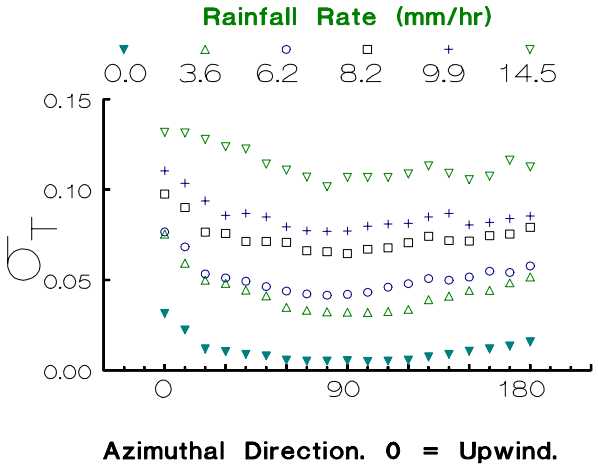

Figure 6. Azimuthal variation of scatterometer measurements from an air- water interface roughened by wind and simulated rains. For all directions, NRCS is a function of rainfall rate.

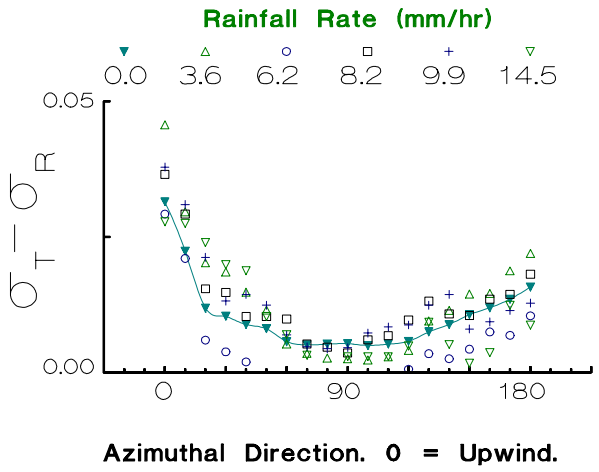

Figure 7. For combined rain and wind conditions, azimuthal dependence of scatterometer measurements after adjustment for rain effects using SRWM-1 with the empirical linear model of the IMST rain simulator. Measurements for wind only case are also shown for comparison. Notice that the vertical resolution is increased by a factor of three compared to Figure 6. For rainy conditions, wind direction as well as wind-speed estimates are feasible using SRWM-1.

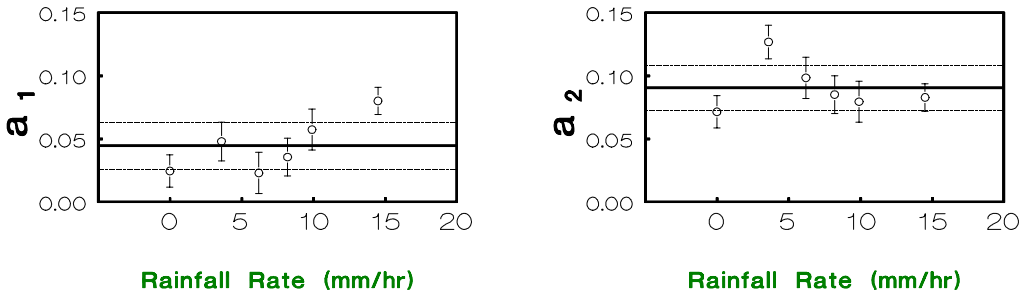

Figure 8. Azimuthal variability of scatterometer cross-section for combined rain and wind conditions is characterized by (a) up-wind/down-wind asymmetry that is quantified by a1 and (b) up-wind/cross-wind asymmetry that is quantified by a2. Vertical lines represent +/- 1 standard deviation of individual coefficient estimates. Horizontal dashed lines represent +/- 1 standard deviation about the group mean values. Light rains do not significantly modify a1 or a2.